PRECISE ACCELERATOR MODELS USING MEASUREMENTS WITH BEAM

F. Zimmermann, CERN, Geneva, Switzerland

Abstract

Precision accelerator models are increasingly important for achieving the design performance of colliders and light sources. An overview is given of procedures and techniques for measuring various parameters of the accelerator model, including the beta function, betatron phase, mismatch, nonlinear detuning, resonance-driving terms, impedance, linear coupling, dispersion, linear and nonlinear chromaticity, momentum compaction, and rf voltage. The complementary model-independent analysis is also discussed. More details and further information may be found in Ref. [1].

1 BETATRON TUNE AND PHASE

The integer part of the betatron tune, $Q = \frac{1}{2\pi} \oint \frac{ds}{\beta(s)}$, may be inferred from a betatron oscillation at injection or the change in closed orbit induced by a steering corrector.

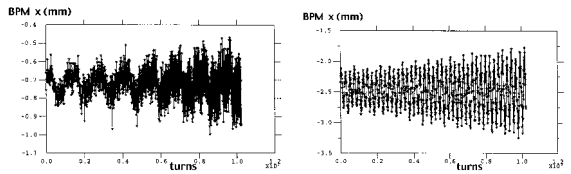

Figure 1: Multi-turn orbit measurement for the motion of the 500th bunch in a train of 1760 bunches at PEP-II. Shown are horizontal BPM orbit readings as a function of turn number: BPM in a dispersive region [left]; BPM in a non-dispersive region [right]. The slow oscillation in the left picture corresponds to energy (or synchrotron) oscillations. The fast oscillation is the betatron motion. (Courtesy U. Wienands, J. Seeman *et al*, 1998.)

After exciting transverse beam motion, the beam position x can be measured on N consecutive turns, as is shown in Fig. 1. The fractional part of the betatron tune then corresponds to the frequency of the largest ψ in the Fourier expansion $x(n) = \sum_{j=1}^{N} \psi(Q_j) \exp(2\pi i n Q_j)$, with an error of the order $|\delta Q| \leq \frac{1}{2N}$.

The resolution is improved by interpolating the shape of the Fourier spectrum around the main peak [2]. For $N \gg 1$, the interpolated tune Q_{Fint} is [2, 3]:

$$Q_{Fint} \approx \frac{k}{N} + \frac{1}{N} \arctan\left(\frac{|\psi(Q_{k+1})|}{|\psi(Q_k| + |\psi(Q_{k+1})|}\right) \quad (1)$$

where $|\psi(Q_k)|$ denotes the peak of the Fourier spectrum, and $|\psi(Q_{k+1})|$ its highest neighbor. For large N the error now decreases as $1/N^2$. Data windowing can further increase the accuracy of the Fourier analysis [3, 4].

From a harmonic analysis of $x(n)$, the betatron phase at the location of the pick up can be determined [5]. The oscillation detected by the kth BPM is $x_{km} = A_k \cos(2\pi Q_x m + \phi_{0,k})$, with m the turn number, and A_k the measured amplitude. In the limit of many turns, N, the betatron phase at the kth monitor is $\phi_{0,k} \approx \tan^{-1}(S_k/C_k)$, where S_k and C_k denote the two Fourier sums $C_k = \sum_{m=1}^{N} x_{km} \cos(2\pi m Q_x)$, and $S_k = \sum_{m=1}^{N} x_{km} \sin(2\pi m Q_x)$. The value of $\phi_{0,k}$ is independent of the amplitude A_k, which may depend on BPM calibration. Phase advances $(\phi_{0,k} - \phi_{0,k-1})$ measured for several beam currents may reveal the transverse impedance distribution around the ring [6, 7], while maximising the amplitude $A_k \approx \sqrt{C_k^2 + S_k^2}$ as a function of Q_x is an alternative way of determining the tune [7].

2 TWISS PARAMETERS

Often in a ring beta functions are measured by detecting the shift of the betatron tune $\Delta_{x,y}$ which results from a change Δk [m^{-1}] in the strength of a quadrupole magnet. The beta function at the quadrupole is given by [8]

$$\beta_{x,y} = \frac{\pm 2}{\Delta k}\left(\frac{1 - \cos(2\pi\Delta_{x,y})}{\tan(2\pi Q_{x,y})} + \sin(2\pi\Delta_{x,y})\right) \quad (2)$$

where $Q_{x,y}$ denotes the unperturbed tune, and the $\pm$ subindex refers to the horizontal and vertical plane, respectively. For small tune changes and far from integer or half integer resonances (*i.e.*, $\cot(2\pi Q_{x,y}) \leq 1$), this can be further simplified to the well known $\beta_{x,y} \approx \pm 4\pi\ \Delta_{x,y}/\Delta k$. A recent beta function measurement at the Fermilab Recycler is depicted in Fig. 2 (left). The nonlinear dependence is well described by the complete Eq. (2). Care has to be taken that the applied change in quadrupole strength does not alter the beam orbit (if the beam is not centered), since otherwise closed-orbit variation at sextupole magnets may affect the tune.

If multi-turn beam position monitors (BPMs) are available, a different and faster measurement extracts the beta function from the betatron phase advance between every three adjacent BPMs [10]. The phase advance ϕ_{fi} from monitor i to monitor f, the optical functions $\beta(s_i)$ and $\alpha(s_i)$, and the transport matrix elements R_{kl} between the two monitors are related by

$$\tan\phi_{fi} = \frac{R_{12}}{R_{11}\beta(s_i) - R_{12}\alpha(s_i)}. \quad (3)$$

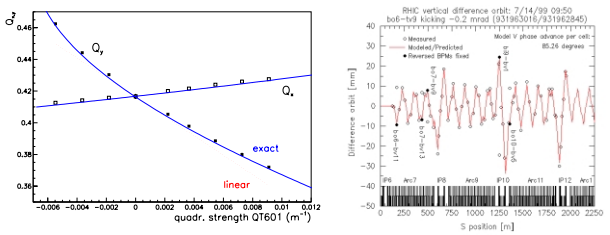

Figure 2: Optics tests. Left: betatron tunes in the Fermilab Recycler Ring are plotted versus the strength of quadrupole QT601 [9]. The measurements [plotting symbols] are compared with theoretical predictions using either the exact nonlinear dependence of Eq. (2) [solid lines], or its linear approximation [dotted lines], and taking the beta functions at quadrupole QT601 to be equal to their design values. Right: difference orbit in RHIC is fitted to the online model [11]. (Courtesy S. Peggs, 2000.)

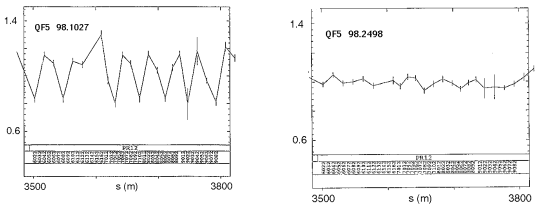

Figure 3: Ratio of the horizontal beta function inferred from phase advance measurements to the model beta function for the PEP-II High Energy Ring (HER): [left] with all magnets at nominal strength; [right] for an increased strength of a single quadrupole pair (QF5) by 0.15%. (Courtesy M. Donald, 1998.)

The phase advance ϕ_{fi} can be inferred from a harmonic analysis, and the coefficients R_{kl} are determined by the design optics assuming that the quadrupole magnets located between the BPMs are at their nominal strength. For a set of three BPMs, there are two independent equations of the form (3), which may be solved for the two remaining unknowns α and β [10]. We denote the transport matrix from BPM 1 to 2 by $\mathbf{M}$ and the matrix from BPM 1 to 3 by $\mathbf{N}$, their respective components by m_{11}, m_{12}, etc., and the phase advance from BPM 1 to 2 (1 to 3) by ϕ_{21} (ϕ_{31}). Applying Eq. (3) twice, the value of β at the first BPM is [10]:

$$\beta(s_1) \;=\; \frac{1/\tan\phi_{21} - 1/\tan\phi_{31}}{m_{11}/m_{12} - n_{11}/n_{12}} \qquad (4)$$

Figure 3 shows an example, where this technique was used to identify a quadrupole gradient error.

One can also infer the beta functions simultaneously at all BPMs by measuring the average (static) orbit response to two, or more, steering correctors [12]. We call x_{ia} and x_{ib} the orbit change measured at the ith BPM when deflections θ_a or θ_b are applied at corrector a or b. The beta

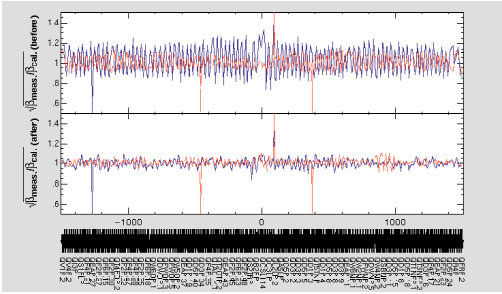

Figure 4: Beta function measurement at KEKB, based on Eq. (5). Ratio of measured β function to the design value is shown before [top] and after optics correction [bottom]. (Courtesy H. Koiso, 2000.)

function is computed from the relation [12]

$$\beta_i = \frac{4\sin^2\pi Q}{\sin^2\Delta}\left(\frac{x_{ia}^2}{\beta_a\theta_a^2} + \frac{x_{ib}^2}{\beta_b\theta_b^2} - \frac{2x_{ia}x_{ib}\cos\Delta}{\sqrt{\beta_a\beta_b}\theta_a\theta_b}\right) \qquad (5)$$

where $\Delta = |\mu_a - \mu_b|$ is the phase advance between the two correctors, which should not be a multiple of π. Prior to applying this equation, the three quantities Δ, θ_a and θ_b are determined by fitting a few BPM readings $x_{ja,b}$ in the vicinity of the correctors to the model optics. The computed beta functions can be verified by exciting other corrector pairs in different sections of the ring and comparing the results. Figure 4 shows an example. Fitting difference orbits to a betatron oscillation is a simpler variant; see Fig. 2 (right).

Yet another method to measure the beta functions exists if BPM and steering corrector are at the same location. The method consists in exciting a corrector, so that it deflects the beam by $\Delta\theta$, and detecting the orbit change $\Delta x_{c.o.}$ at the associated BPM [13]. Assuming the beam energy is unchanged, the beta function at the BPM is $\beta_{\rm BPM/cor} \approx 2\,\tan\pi Q\,\Delta x_{c.o.}/\Delta\theta$.

An elegant procedure is available to control the beta function at a local symmetry point, such as the interaction point of a collider ring. A pair of symmetrically placed quadrupoles is excited with opposite sign by an amount $\pm\Delta k$. The total tune shift is $\Delta Q_{\rm tot} = \approx \Delta k\,[<\beta_+> - <\beta_->]/(4\pi)$, where $< \ldots >$ indicates the average over the quadrupole, and the $\pm$ sign refers to the left or right quadrupole. The optics is perfectly adjusted, if $\Delta Q_{\rm tot} = 0$. The beta function at the collision (symmetry) point β^* is a quadratic function of the ratio $\eta = 4\pi\ \Delta Q_{\rm tot}/\Delta k$ of the form [14] $\beta^* = \beta^*_{\rm design}\left(1 + a_{\rm optics}\eta^2\right)$, where $\beta^*_{\rm design}$ is the nominal beta function, and the coefficient $a_{\rm optics}$ can be obtained from an optics calculation.

In a transport line (or linac) the beta function does not only depend on the beam-line elements but also on the incoming beam parameters. To match the beam line optics to the incoming beam, two procedures are frequently used: multi-wire (or multi-screen) beam-size measurements and quadrupole scans. The mathematical algorithm for either

case expresses the transverse beam sizes $\sigma_x^{(l)}$, corrected for dispersion and energy spread, in terms of the α and β functions and the emittance at an upstream location s_0. To simplify the notation, we introduce a vector containing the n measured beam sizes $\Sigma = (\sigma_x^{(1)2}, ..., \sigma_x^{(n)2})$, the 3-component vector of unknown beam parameters at location s_0, $\mathbf{o} = (\beta(s_0)\epsilon, -\alpha(s_0)\epsilon, \gamma(s_0)\epsilon)$, and the $n \times 3$ matrix $\mathbf{B}$ whose ith row reads $B_i = (R_{11}^{(i)2}, 2R_{11}^{(i)}R_{12}^{(i)}, R_{12}^{(i)2})$, where R_{kl} is the (k,l) transport matrix element from s_0 to the location of the ith beam-size measurement. The equation connecting Σ, $\mathbf{B}$ and $\mathbf{o}$ is $\Sigma_x = \mathbf{B} \cdot \mathbf{o}$, with the least-square solution $\mathbf{o} = (\hat{\mathbf{B}}^T \cdot \hat{\mathbf{B}})^{-1} \cdot \hat{\mathbf{B}}^T \cdot \hat{\Sigma}_x$, where $\hat{\Sigma}_x^{(l)} = \Sigma_x^{(l)}/\sigma_{\Sigma_x^{(l)}}$, $\hat{\mathbf{B}}_{li}^{(l)} = \mathbf{B}_{li}^{(l)}/\sigma_{\Sigma_x^{(l)}}$, and $\sigma_{\Sigma_x^{(l)}}$ the rms error of $\Sigma_x^{(l)}$. The errors of the parameters $\mathbf{o}$ are $\sigma_{o_i} = \sqrt{(\hat{\mathbf{B}}^T \cdot \hat{\mathbf{B}})^{-1})_{ii}}$. The three quantities ϵ, β, and α are inferred from $\epsilon = \sqrt{o_1 o_3 - o_2^2}$, $\beta = o_1/\epsilon$, and $\alpha = -o_2/\epsilon$. The deviation of β, α, and γ from the design parameters β_0, α_0 and γ_0 is characterised in terms of a so-called 'Bmag' (β matching) parameter [15, 16]: $\mathrm{Bmag} = (\beta\gamma_0 - 2\alpha\alpha_0 + \gamma\beta_0)/2$. If an unmatched beam is injected into a ring or linac, it will filament until the beam distribution approaches a shape that is matched to the lattice. After complete filamentation, the emittance is given by the product of Bmag and the initial ϵ. Once the values of β and α are known, quadrupole magnets can be adjusted in order to match the optical functions at a selected point to their design value, so that Bmag=1; see, *e.g.*, Ref. [17]. In addition, the procedure provides an absolute measure of the emittance. Finally, groups of magnets that are combined into linear [18] or nonlinear [19] orthogonal tuning 'knobs' allow for an empirical optics correction.

3 LINEAR COUPLING

Linear coupling of horizontal and vertical betatron motion may decrease the dynamic aperture and, in electron colliders or light sources, it degrades the luminosity or brilliance. A standard method to globally correct the linear betatron coupling in a storage ring [20, 21] is to minimise the distance κ_- of closest tune approach, by varying skew-quadrupole correctors. The coupling strength κ_- can also be inferred from the modulation amplitude and modulation period in the beam response to a kick [20, 21]. In addition, to achieve optimum vertical beam emittances in electron or positron rings, it often is necessary to identify and correct local coupling sources. One approach here is to measure the cross-plane orbit response, *e.g.*, the vertical orbit changes due to horizontal closed orbit bumps in different sections of the ring [22].

4 NONLINEAR OPTICS

Nonlinear magnetic fields induce a tune shift with amplitude, and they excite higher-order resonances, which are visible as additional lines in the tune Fourier spectrum. The resonance $kQ_x + lQ_y = p$ (k, l, and p integers) gives rise to lines at $(k \pm 1)Q_x + lQ_y$ in the horizontal spectrum. From amplitude, phase and frequency of the various spectral lines the dominant nonlinearities affecting the beam motion can be reconstructed [23,24]. An example is shown in Fig. 5. The nonlinearities may also be probed by adiabatically exciting large coherent betatron oscillations using an ac dipole [26]. This method will be tested at RHIC.

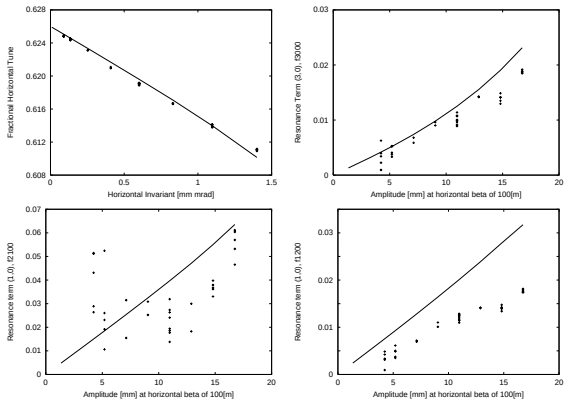

Figure 5: Detuning and first-order resonance driving terms, measured at the SPS [25]. Shown are the betatron tune [top left] and the relative amplitude of several resonance lines with respect to the main tune line [other] as a function of the oscillation amplitude. Plotting symbols are experimental data; lines are from a tracking simulation. 170 turns were sampled per point. (Courtesy F. Schmidt, 2000.)

5 DISPERSION

In most storage rings the dispersion function is inferred from the orbit change Δx induced by a shift in rf frequency. A frequency shift Δf_{rf} changes the relative energy by $\delta = -(\alpha_c - \gamma^{-2})^{-1}\ \Delta f_{\mathrm{rf}}/f_{\mathrm{rf}} \approx -1/\alpha_c\ \Delta f_{\mathrm{rf}}/f_{\mathrm{rf}}$. The last approximation ignores the change in particle velocity and is valid for electron rings. The dispersion is $\eta(s) = \left(\gamma^{-2} - \alpha_c\right)\ \Delta x(s)/(\Delta f_{\mathrm{rf}}/f_{\mathrm{rf}})$. As an illustration, Fig. 6 (left) shows a dispersion measurement at the PEP-II HER. At LEP, a different 'dynamic' dispersion measurement has been applied [5], where the phase of the rf voltage is harmonically modulated at a frequency close to the synchrotron frequency and the frequency component of the induced (resonant) orbit variation at the synchrotron frequency is used to infer the dispersion function at each BPM. If the dispersion at the cavities is nonzero, the dynamic measurement will give a result different from the static measurement [27]. Similar dynamic schemes have been tested at the SLC and ATF damping rings. In both these rings, a longitudinal oscillation is induced by a shock excitation: either a sudden step-change to the rf voltage (at the SLC [28]) or a fast phase jump (at the ATF [29]). The two methods can also give spurious results.

In a transport line, or linac, the linear and nonlinear dispersion at location s is written as $\Delta x(s) = R_{16}(s)\delta + T_{166}(s)\delta^2 + U_{1666}(s)\delta^3$ where the 2nd and 3rd order contributions are characterised by $T_{166}(s)$ and $U_{1666}(s)$. These terms can be measured via a shift in beam energy. Re-

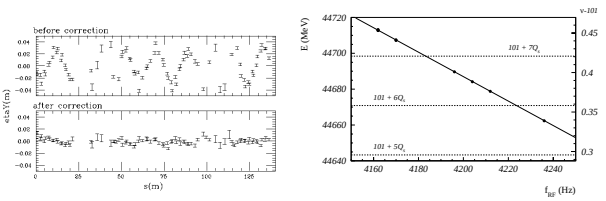

Figure 6: Left: Vertical dispersion measured via $\pm$5-kHz rf frequency ramp at the KEK ATF Damping Ring before [top] and after correction [bottom]; a dispersion of $\eta = 5$ mm corresponds to an orbit change of $\Delta x \approx 15$ μm. (Courtesy J. Urakawa, 2000). Right: Change of beam energy, E, as a function of the rf frequency, $f_{\rm rf}$, in LEP [35]. Only the last four digits of the rf frequency are shown (the nominal value is $f_{\rm rf} = 352\ 254\ 170$ Hz). Strong spin resonances are indicated by dotted lines. From this measurement the momentum compaction factor was determined to be $(1.86 \pm 0.02) \times 10^{-4}$, comparing well with the calculated value of 1.859×10^{-4}. (Courtesy R. Assmann, 1998).

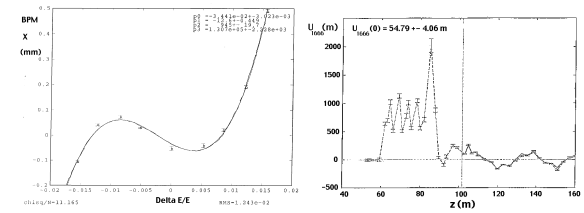

Figure 7: Third order dispersion in the SLC ring-to-linac transfer line (RTL) [30]: Left: BPM reading vs. beam energy. Right: 3rd order dispersion inferred for all BPMs in the RTL and in the early linac; the 3rd order dispersion in the linac is fitted to calculate the magnitude of the U_{1666} and U_{2666} matrix elements. (Courtesy P. Emma, 1998.)

sults are illustrated in Figure 7 for the North ring-to-linac transfer line (RTL) of the SLC. The left picture shows the beam position at one of the RTL BPMs as a function of the beam energy. The cubic dependence indicates a large 3rd order dispersion, whose value was obtained from a polynomial fit. Plotted in the right picture is the 3rd order dispersion function so determined as a function of position along the RTL and in the early part of the SLAC linac. In 1991 two octupole magnets were installed in order to cancel the U_{1666} term. The optimum octupole strength, found by minimising the linac emittance as a function of the octupole excitation, and the corresponding U_{1666} value are in good agreement with the 3rd order dispersion inferred from the BPM readings [1, 30]. Also linear (and second order) dispersion requires correction [17]. In a linear collider, the beam dispersion, *i.e.*, the energy-position correlation within the bunch, must be controlled. This can be done using (tilted) wire scanners at dispersive locations [31].

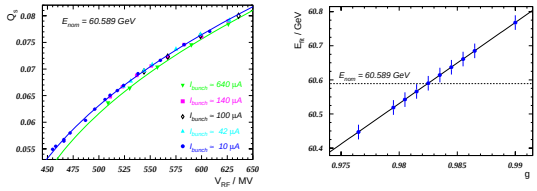

Figure 8: Left: Q_s as function of total rf voltage in LEP; the two curves are fits to the 640 μA and 10 μA data. The difference due to parasitic mode losses is clearly visible [36]. Right: beam energy fitted from Q_s vs. $V_{\rm rf}$ measurement as a function of rf voltage calibration factor g; the dotted line indicates the known energy value [36]. (Courtesy A.-S. Müller, 2000).

6 LONGITUDINAL OPTICS

If the rf voltage is well known, the momentum compaction factor α_c can be inferred directly from the synchrotron tune. For an electron ring one can remove the dependence on the rf voltage by also measuring bunch length, quantum lifetime, and/or the rms energy spread [32]. At the KEKB linac, a streak camera synchronised with the injector rf system was used to monitor the electron path length as a function of energy, and, thereby, the first and second order momentum compaction factor [33]. For unbunched proton beams, the momentum compaction factor, $\alpha_c = -(\Delta B/B)/(\Delta T/T)$, follows from the change in revolution period T with bending field B, which can be detected by a Schottky monitor [34]. Extremely accurate measurements of the momentum compaction were performed at LEP. Here the beam energy is determined using resonant depolarisation. The resonant spin tune ν_0 depends linearly on beam energy, $\nu_0 = a_e\gamma = \frac{E\ [\mathrm{MeV}]}{440.6486(1)\ [\mathrm{MeV}]}$, with a_e the electron anomalous magnetic moment. Beam-energy measurements for different rf frequencies determine α_c; see Fig. 6 (right). Measuring the synchrotron tune Q_s as a function of rf voltage $V_{\rm rf}$, for various beam currents, and fitting to $Q_s^2 = \frac{\alpha_C h}{2\pi}\left(\frac{g^2e^2V_{rf}^2}{E_c^2} + Mg^4V_{rf}^4 - \frac{1}{E_c^2}\tilde{U}_0^2\right)^{1/2}$, where the V_{rf}^4 term accounts for the rf distribution, yields the longitudinal loss factor as $\tilde{U}_0$; see Fig. 8 (left). From this fit also α_c was determined with a precision better than 10^{-3} [36]. In addition, if the beam energy is known at one point, *e.g.*, on a spin resonance, the Q_s vs. $V_{\rm rf}$ curve can calibrate the rf voltage (Fig. 8 right) [36].

7 CHROMATICITY

The chromaticity is normally determined by measuring the tune shift as a function of the rf frequency $f_{\rm rf}$.: $\xi_{x,y} = \frac{\Delta Q_{x,y}}{\Delta p/p} = \left(\gamma^{-2} - \alpha_c\right)\frac{\Delta Q_{x,y}}{\Delta f_{\rm rf}/f_{\rm rf}}$. An example from LEP is shown in Fig. 9 (left).

A fast chromaticity measurement was developed at CERN in preparation for LHC [37]. After applying a transverse kick, the betatron phase shift $\Delta\phi_\beta$ between bunch head and tail, separated in time by $\Delta\tau$, is measured over n turns. The chromaticity follows from $\xi_{x,y} =$

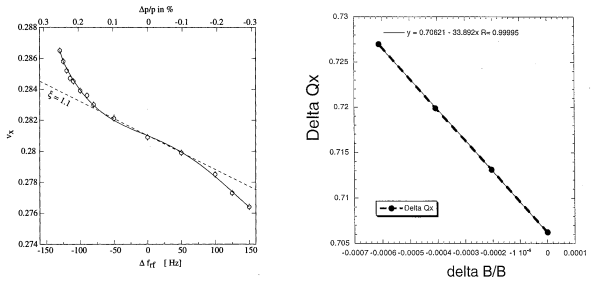

Figure 9: Chromaticity measurements. Left: Horizontal tune as a function of the rf frequency in LEP. Plotting symbols with error bars are the data. The dashed line is the linear chromaticity as calculated from tune measurements at $\Delta f_{\rm rf} = \pm 50$ kHz. (Courtesy H. Burkhardt, 1998.) Right: Natural chromaticity in the PEP-II HER. Shown is the horizontal tune vs. the relative change in the main dipole field. (Courtesy U. Wienands, J. Seeman *et al*, 1998.)

$-\left(\alpha_c - \gamma^{-2}\right)\ \Delta\phi_\beta(n)/\left[Q_{x,y}\omega_0\ \Delta\tau(\cos(2\pi n Q_s) - 1)\right]$.

Another interesting optics test is to measure the natural chromaticity, which is the chromaticity the ring would have without sextupole magnets, by detecting the variation of the betatron tune as a function of the bending field. Since the rf frequency is unchanged, the orbit in the sextupoles remains approximately constant. The absolute beam energy changes in proportion to the field, and the natural chromaticity $\xi_{x,y}^{nat}$ is given by $\xi_{x,y}^{nat} \approx \Delta Q_{x,y}/(\Delta B/B)$. A typical result is depicted in Fig. 9 (right). Beta functions measured at different rf frequencies reveal the local chromaticity. In addition, the tunes measured for several sextupole strengths as a function of rf frequency follow curves which approximately intersect in a single point. At this 'central rf frequency' the orbit on average passes through the center of all sextupoles [38, 39]. This is useful to monitor circumference and beam energy [40, 41].

8 DATA ANALYSIS TECHNIQUES

If the beam response to a large number of steering correctors is measured at all BPMs, many parameters can be adjusted in an off-line accelerator model so as to best reproduce the observed response matrix. A good example is the LOCO code [42].

Singular value decomposition (SVD) is a powerful tool with a broad range of applications, such as reducing the strengths of orbit correctors [43], creating orthogonal tuning knobs [44], or analysing BPM data [45]. Least-square fits do not always give correct results, and sometimes they must be substituted by a principal-axes transformation [46].

Model-independent analysis [45] extracts temporal and spatial patterns from an arbitrary series of beam data, identifies the physical variables contributing to beam motion, and, *e.g.*, was used to localise linac wake-field sources.

9 SUMMARY

Many procedures have been developed for verifying or updating the accelerator model.

ACKNOWLEDGEMENT

Many people kindly provided help and material, in particular R. Assmann, C. Bovet, H. Burkhardt, Y. Cai, J. Corbett, M. Donald, P. Emma, M. Giovannozzi, K. Hanke, A. Hofmann, B. Holzer, J. Klem, H. Koiso, M. Minty, A.-S. Müller, S. Peggs, N. Phinney, I. Reichel, R. Jones, F. Ruggiero, J. Safranek, H. Schmickler, F. Schmidt, J. Seeman, J. Urakawa, W. Wan, D. Whittum, & U. Wienands.

REFERENCES

[1] F. Zimmermann, Joint Acc. School on 'Beam Measurement' Montreux (1998).
[2] E. Asseo, CERN PS/85-3 (LEA) (1985).
[3] R. Bartolini, et al., Proc. EPAC 96, p. 1329 (1996).
[4] F. J. Harris, Proc. IEEE Vol. 66, No 1, January 1978.
[5] J. Borer, e al., Proc. of EPAC92, p. 1082 (1992).
[6] D. Brandt, et al., Proc. IEEE PAC 95, Dallas, p. 570 (1995).
[7] J. Klem, CERN SL seminar on 23.03.00.
[8] K. Oide, private communication (1997).
[9] W. Wan and F. Zimmermann, March 4, 2000, unpublished.
[10] P. Castro, CERN SL/Note 92-63 (1992).
[11] S. Peggs, private communication (2000).
[12] N. Akasaka, H. Koiso, et al., unpublished (1999).
[13] J. Corbett, private communication (1998).
[14] C. Bovet, in J. Bosser (ed.), CERN-PE-ED 001-92.
[15] M. Sands, SLAC-AP-85 (1991).
[16] W. Spence, private communication (1996).
[17] K. Hanke et al., PAC99, p. 1282 (1999).
[18] K. Hanke et al., PAC99, p. 1285 (1999).
[19] N. Walker et al., PAC93 Washington, p. 95 (1993).
[20] P. Bryant, CERN Accelerator School, CERN 89-05 (1989)
[21] F. Willeke, G. Ripken, DESY 88-114 (1988).
[22] J. Urakawa et al., unpublished (2000).
[23] C.-X. Wang and J. Irwin, SLAC-PUB-7547 (1997).
[24] R. Bartolini and F. Schmidt, Part. Accelerators (1997).
[25] R. Bartolini et al., Proc. IEEE PAC99 New York, p. (1999).
[26] M. Bai et al., Phys. Rev. E 56, p. 6002 (1997).
[27] F. Ruggiero, CERN SL/91-38 (1991).
[28] M. Minty, unpublished (1997).
[29] K. Kubo and T. Okugi, ATF Report ATF-97-19 (1997).
[30] P. Emma and W. Spence, KEK Proceedings 92-6 (1992).
[31] P. Emma et al., SLAC-PUB-6208 (1993).
[32] U. Wienands, private communication (1998).
[33] H. Koiso and K. Oide, private communication (1998).
[34] A. Hofmann, private communication (1998).
[35] R. Assmann, *et al.*, CERN-SL/95-02 (1995).
[36] A.-S. Müller, Ph.D. thesis, U. Mainz, and these proceedings (2000).
[37] D.Cocq, O.R.Jones, H.Schmickler, 8th Beam Instr. Workshop BIW'98, Stanford, CA, USA (1998).
[38] A. Piwinski, *et al.*, measurements at DORIS-I and HERA.
[39] For LEP this measurement was proposed by A. Hofmann.
[40] C. Zhang, et al., HEACC'92, Hamburg, p. 409 (1992).
[41] H. Schmickler, CERN LEP performance note 89 (1993).
[42] J. Safranek, Nucl. Instr. and Meth. A388, 27 (1997).
[43] V. Ziemann, SLAC CN-393 (1992).
[44] P. Raimondi, private communication (1998).
[45] J. Irwin *et al.*, PRL 82, p. 1684 (1999).
[46] T. Lohse, P. Emma, SLAC CN-371 (1989).